Interactive Simulation and Visualization of Lamb Wave Propagation in Isotropic and Anisotropic Structures

J. Moll[1], C. Rezk-Salama[2], R.T. Schulte[1], T. Klinkert[3], C.-P. Fritzen[1] and A. Kolb[3]

[1]Institute of Mechanics and Control Engineering - Mechatronics, University of Siegen, Germany
[2]Mediadesign University of Applied Science Düsseldorf, Germany
[3]Computer Graphics and Multimedia Systems, University of Siegen, Germany

E-mail: moll@imr.mb.uni-siegen.de

Abstract. Structural health monitoring systems allow a continuous surveillance of the structural integrity of operational systems. As a result, it is possible to reduce time and costs for maintenance without decreasing the level of safety. In this paper, an integrated simulation and visualization environment is presented that enables a detailed study of Lamb wave propagation in isotropic and anisotropic materials. Thus, valuable information about the nature of Lamb wave propagation and its interaction with structural defects become available.

The well-known spectral finite element method is implemented to enable a time-efficient calculation of the wave propagation problem. The results are displayed in an interactive visualization framework accounting for the human perception that is much more sensitive to motion than to changes in color. In addition, measurements have been conducted experimentally to record the full out-of-plane wave-field using a Laser-Doppler vibrometry setup. An aluminum structure with two synthetic cuts has been investigated, where the elongated defects have a different orientation with respect to the piezoelectric actuator. The resulting wave-field is also displayed interactively showing that the scattered wave-field at the defect is highly directional.

1. Introduction

Structural Health Monitoring (SHM) has gained more and more attention during the last 20 years. In the beginning mostly vibration-based techniques were employed for global monitoring while conventional non-destructive testing (NDT) methods based on ultrasonic waves have been used on a more local level. In parallel, the wave-based techniques have been combined with permanently installed sensors and thereby adopted to the concept of SHM. The associated short wavelengths of the ultrasonic waves lead to measurable wave scattering even at small discontinuities.

Lamb waves, also known as guided plate waves, are a type of ultrasonic waves that remain guided between two parallel free surfaces, such as the upper and lower surfaces of a plate or shell. In recent years, Lamb waves have shown great potential in SHM applications to detect damage in plate-like structures, e.g. holes [1] and cracks [2]. They can travel over long distances and thus cover large areas with only a limited number of piezoelectric transducers. The excitation of Lamb waves forces at least two modes to propagate across the structure simultaneously, i.e.

the S_0-mode and the A_0-mode. Here, the S_0-mode represents mainly the longitudinal and the A_0-mode predominantly the transverse wave motion. This property shows the multi-modal characteristics of Lamb waves. In contrast to isotropic plates the wave propagation becomes much more complicated in anisotropic structures which are often used in modern aircrafts. Here, the wave propagation depends not only on the plate thickness and the excitation frequency: Wave velocity and peak-to-peak amplitude are also nonlinear functions of the wave propagation direction [3] and [4].

An important challenge of SHM is to find the location of possible damages based on the signal readings from a limited number of sensor positions. Having recorded a large number of measurements by the sensor array or a scanning Laser vibrometer, SHM systems require fast data analysis and visualization. Due to their high memory bandwidth and the parallel execution model, modern graphics processing units (GPUs) are ideal candidates to efficiently perform data processing and visualization tasks. In this paper, we are presenting a fast, integrated simulation and visualization system based on Lamb wave propagation. The benefit in such a system is the ability to directly modify user-specified parameters of the simulation and immediately observe the results in the visualization system. It allows a fast workflow for the evaluation of different actuator/sensor-configurations.

System Overview
We propose a system which performs simulation and visualization in parallel. Such a system will support user interaction for both the Lamb wave simulation and the visual display of the wave-field data. A commodity desktop computer is equipped with one multicore central processing unit (CPU) as well as one graphics processing unit (GPU). High run-time performance for our system requires the utilization of all available computing resources in parallel. In our system the Lamb wave simulation is implemented in C++ for efficient execution on a single CPU. Each time step calculated by the CPU is immediately transferred from main memory to local video memory for visualization autonomously performed by the GPU. The user is thus able to immediately display the visualization results of each time step in a running simulation. He can modify the visual representation of the data while the simulation is still running. Whenever the user decides to change simulation-related parameters (such as the sensor positions), the simulation process may be restarted without affecting the visualization subsystem.

The remainder of the paper is organized as follows. Section 2 provides an overview of previous works related to our system. In contrast to others, the application of the so called spectral element method allows us to efficiently simulate different sensor array configurations as described in section 3.1, and analyze the results visually and interactively as shown in section 3.2. Such an integrated simulation and visualization workflow with the human in the loop provides excellent opportunities for gaining insights into the nature of Lamb wave propagation. Section 4 describes the experimental setup for recording the wave-field data with a Laser-Doppler vibrometer. The results are presented in section 5 where a special focus is on the interaction of the incident ultrasonic wave with different types of defects. The paper ends with a discussion of the proposed visualization methodology in section 6 and the conclusions.

2. Related Work

Analyzing the non-stationary ultrasonic sensor signals requires a profound understanding of the wave propagation and the interaction with various types of defects. This is particularly important for the damage localization problem. Hence, much work has been done in recent years to simulate propagating waves. Among others the finite difference method (FDM) [5], the pseudospectral method (PSM) [6], the finite element method (FEM) [7], the boundary element method (BEM) [8] and the local interaction simulation approach (LISA) [9] are widely used.

A very promising method is the spectral element method (SEM) that was first proposed by Patera [10]. It combines the accuracy of the global pseudospectral method with the flexibility of the FEM. However, in the context of high frequency wave propagation in thin shell structures extensive use of this technique has started just few years ago [11], [12], [13], [14].

Other researchers have used Laser-Doppler vibrometry to analyze the wave propagation phenomena experimentally. A basic study has been conducted in [15] where the authors compare ultrasonic signals recorded by laser measurements with those from piezoelectric transducers. In that study, a good agreement has been found between the sensor responses. Information about the in-plane components of the wave-field become available by a three-dimensional laser setup which is used in [16] for impact damage detection in composite structures. Measuring the surface velocities over a defined grid yields the so called full wave-field data. The resulting huge datasets have been processed in [17] by a two-dimensional Fourier transform in order to remove the incident wave components. The goal of that study is to reveal the low-amplitude reflections coming from the interaction with the defect which are often masked under the high amplitude of the incident waves.

The visualization of acoustic wave-fields have been been performed for example by the authors in [18], [19] and [20]. All the techniques have in common that the wave propagation is done forward in time without interactive functionalities. Apart from SHM, Schultz et al. [21] present a visualization approach for carbody vibration and sound wave simulation within the car interior. For many different application scenarios, integrated simulation and visualization systems, such as the one proposed in [22] have gained much attention in recent years. The ability to modify simulation parameters and interactively examine the results provides significant benefits with respect to an efficient scientific workflow with the human in the loop.

3. Theory

3.1. Spectral shell elements for the simulation of wave propagation

Short wavelengths are beneficial for detecting small defects, because the detectable damage size is directly related to the wavelength. Thus, conventional finite element simulations become computationally inefficient, because a very dense mesh grid is required. Consequently, the spectral element method (SEM) is used in this paper. While modeling of Lamb waves requires a full 3D-model in theory, a 2D-approach can be used with certain accuracy [18].

The Gauss-Lobatto-Legendre (GLL) spectral element discretization based upon quadrangular elements proceeds as follows: a mesh of n_{el} non-overlapping elements Ω^e is defined on the domain Ω. These elements are subsequently mapped individually on a reference element $\Omega^{ref} : \xi \in$ [-1,1] x $\eta \in [-1, 1]$ using an invertible local mapping. On each element a set of GLL nodes is defined. Within the reference element these nodes are the (N+1) roots of the polynomials (1-ξ^2)$P'_{N-1}(\xi)$=0 and (1-η^2)$P'_{N-1}(\eta)$=0 , where P'_{N-1} denotes the first derivative of the (N-1)-*th* order Legendre polynomial. In contrast to classical finite elements the distribution of nodes is irregular.

The spectral shell element is based on the first order shear deformation theory (FSDT) with out-of-plane displacement w, independent rotations θ_x and θ_y and in-plane displacements u and v. The basic equations of motions resulting from this theory are documented in many textbooks, e.g. [23]. On the nodal base defined above, Lagrange interpolation polynomials can be used as

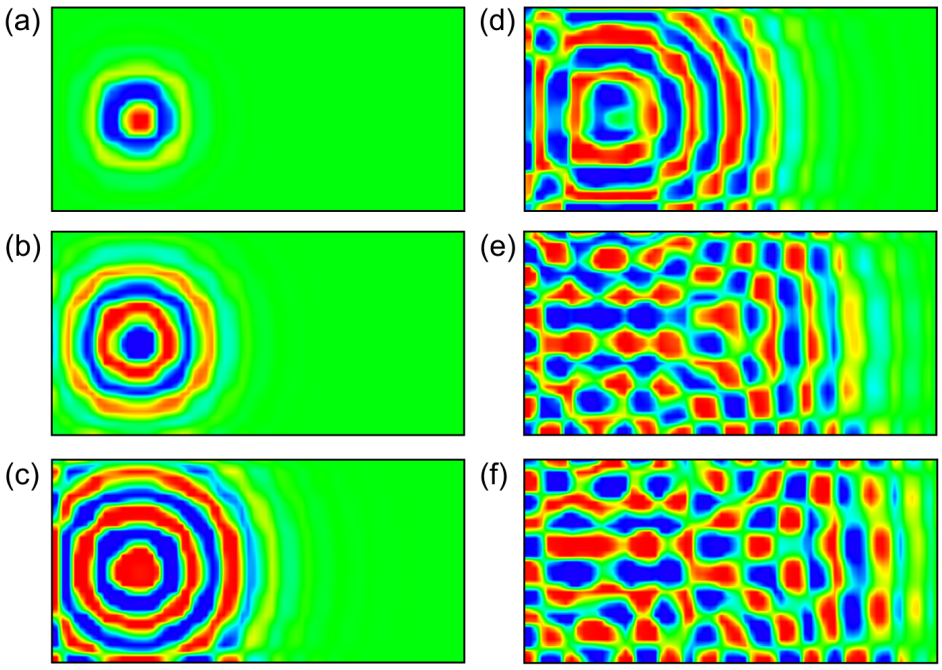

Figure 1. Different time steps from a Lamb wave simulation. The out-of-plane displacement field is color-coded in HSV color space.

shape functions, leading to an expression for the displacement field of the following form:

$$\begin{bmatrix} w(\xi,\eta) \\ \theta_x(\xi,\eta) \\ \theta_y(\xi,\eta) \\ u(\xi,\eta) \\ v(\xi,\eta) \end{bmatrix} = \sum_{i=1}^{N+1} \sum_{j=1}^{N+1} \psi_i(\xi) \cdot \psi_i(\eta) \begin{bmatrix} \hat{w}(\xi_i,\eta_j) \\ \hat{\theta}_x(\xi_i,\eta_j) \\ \hat{\theta}_y(\xi_i,\eta_j) \\ \hat{u}(\xi_i,\eta_j) \\ \hat{v}(\xi_i,\eta_j) \end{bmatrix} \tag{1}$$

Here, $\psi_i(\xi)$ denotes the i-th 1D Lagrange interpolation function and the hat indicates nodal degrees of freedom. An important property of these interpolation polynomials is the discrete orthogonality $\psi_i(\xi) = \delta_{ij}$, where δ_{ij} denotes the Kronecker delta. By utilizing this kind of shape functions based on the GLL-nodes, the highest interpolation accuracy is achieved [24]. This leads to the advantage, that only five to six nodes (depending on the degree of the interpolation polynomial) per shortest wavelength are necessary to capture the structural behaviour with the same accuracy compared to 15-30 nodes, which are needed using lower order FE [25]. Derivation of the weak form and the assembly of mass- and stiffness matrix follow standard FE procedures. Details about these matrices can be found in [14]. For the general case of anisotropic laminates, this formulation leads to an optimally concentrated, but non-diagonal mass matrix because of coupling terms between in-plane and rotational degrees of freedom. Fortunately, in almost every application, laminates with symmetrical layup are used where the coupling coefficients vanish. In this situation, the discrete orthogonality of the shape functions in conjunction with the application of the Gauss-Lobatto integration rule for the numerical integration of element matrices leads to a diagonal mass matrix. By using the central difference scheme the resulting system of equations can be solved very rapidly without matrix decomposition.

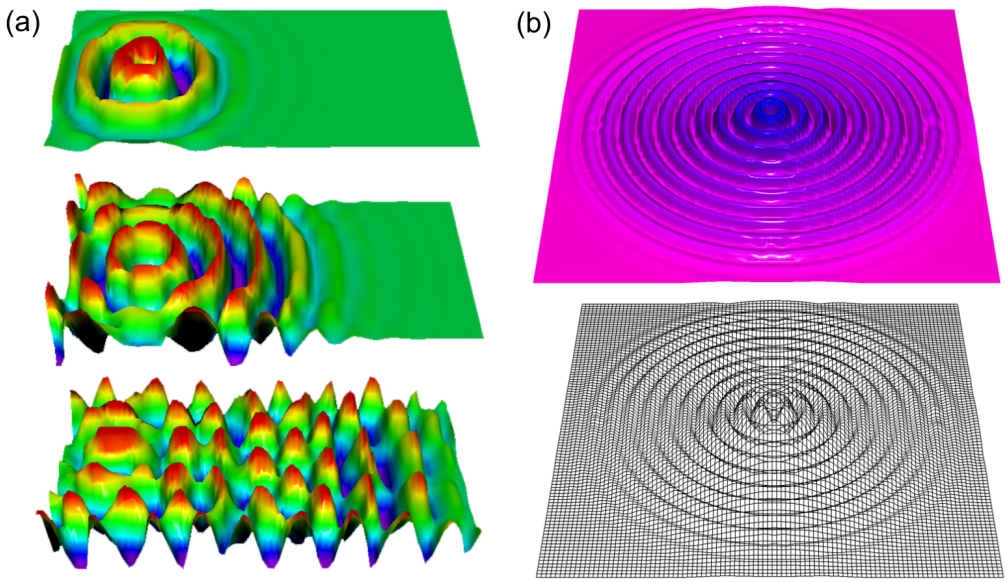

Figure 2. (a) Different time steps from the Lamb wave simulation. The plate geometry is deformed by the amplified out-of-plane displacement. (b) Deformed plate geometry with local illumination (top) and wireframe display (bottom).

3.2. Visualization

The result of the aforementioned simulation step is a time-dependent two-dimensional displacement field that describes the wave propagation in the underlying plate. The subsequent visualization step maps the resulting time series on top of a corresponding polygonal model of the plate's geometry. The most straightforward way to display the simulation data is color-coding of the wave-field characteristics as shown in Figure 1. While the simulation of a time step is extremely fast, it can be easily calculated and displayed on-the-fly. However, since the simulation of one time step requires knowledge about the previous time step, on-the-fly simulation will prohibit the user to jump back and forth in time without having to rerun this simulation from the beginning. Therefore, we use a data structure, i.e. a 3D texture, to cache previously calculated time steps at certain intervals. Each n-th discrete time step of the time-dependent simulation is stored as a single slice of a 3D texture image. Two dimensions cover the spatial coordinates of the plate with respect to the tessellation into spectral elements, and the third axis represents the discrete time steps. Throughout our experiments, however, subtle changes in wave characteristics such as low amplitude reflections turned out to be hard to notice with a color-coded display alone. Human perception is much more sensitive to motion than to changes in color [26]. To provide the user with additional visual cues we display the amplitude of the wave as a highly exaggerated deformation of the plate geometry. A similar idea has been followed by Schultz et al. in order to visualize sound waves in the interior of a car [21]. We implemented this idea using a time-dependent displacement map extracted on-the-fly from the 3D texture. Amplitude and phase of the wave is used to calculate the amount of displacement, see Figure 2a. The original polygonal plate geometry is subdivided into small patches with a resolution equal to or less than the size of the spectral elements used during the simulation. As already mentioned, this discretization is a function of the underlying wavelength. On modern graphics boards, such tessellation tasks can be easily performed on-the-fly using so-called geometry shaders. However, since our subdivision is static we opt for a tessellation of

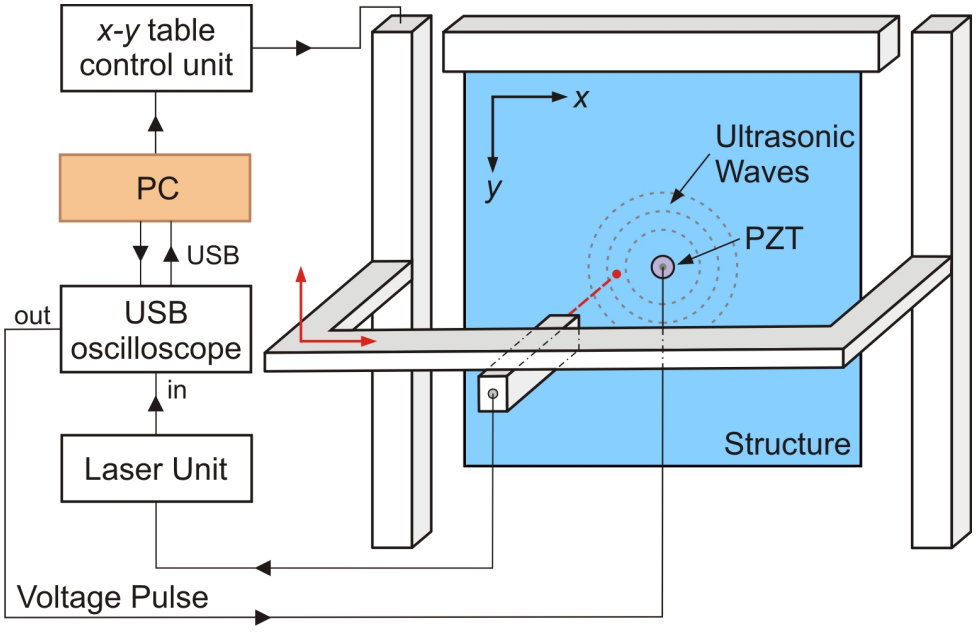

Figure 3. Laser vibrometry setup to scan a plate-like structure automatically.

the geometry in a pre-processing step. At run-time a customized vertex program calculates the amount of displacement from the wave characteristics sampled from the 3D texture. Local illumination techniques are important for the perception of shape and small-scale structures. Most illumination models rely on normal vectors that can be approximated by directional derivatives of the displacement field using central differences. The derivative in direction of both, the local tangent and the binormal of the undistorted surface, allows us to calculate a deformed surface normal in the tangent space of the polygon. This normal vector estimated on-the-fly is used subsequently to calculate traditional Blinn-Phong illumination with a variable light position [27]. A high shininess exponent will lead to crisp specular highlights and significantly increase the perception of shape and motion, compare Figure 2b. As described above, the inputs of the simulation are the mass- and stiffness matrices of the spectral elements, as well as the location of the piezoelectric actuator. Modifications of these parameters will require rerunning the simulation from the beginning.

4. Experimental Setup

Figure 3 shows a schematic of the laser vibrometry setup which is used in this paper to measure point-wise and noncontactly the out-of-plane wave-field generated by a piezoelectric actuator. The system comprises five major elements namely a PC, a USB oscilloscope, a laser unit, a motorized x-y table and the structure with a single surface mounted piezoelectric transducer (PZT). When a narrowband voltage pulse is sent towards the PZT an ultrasonic wave starts to propagate across the structure. The resulting particle velocities as a function of time can be recorded at each coordinate (x,y) using the laser system. A motorized x-y table that is controlled by the PC positions the laser in order to scan the whole structure point-by-point. The optical signal coming from the laser is converted to an electrical signal by the laser unit. A USB oscilloscope samples this analogue signal with a sampling frequency of $10 MHz$. In a final step, the data are transferred to the PC for offline post-processing.

In the experimental part of this paper a squared isotropic aluminum plate with the dimensions $600mm$ x $600mm$ x $1.5mm$ is considered, see Figure 4. A circular PZT with a diameter of $10mm$

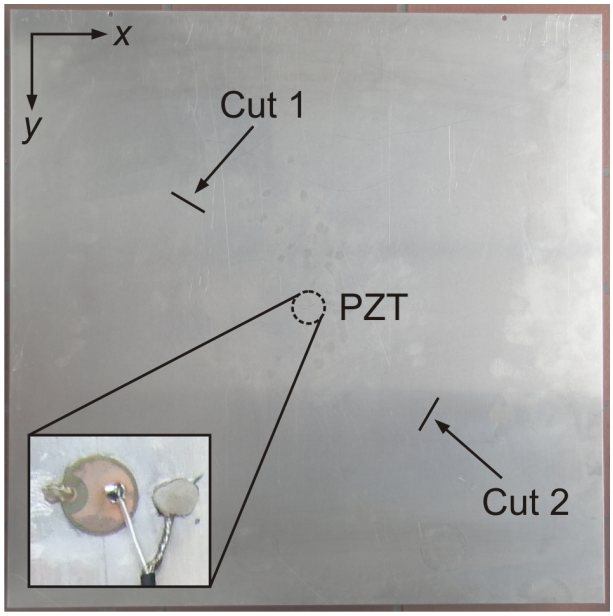

Figure 4. Aluminum structure with two $40mm$ long cuts at different spatial positions and different orientation with respect to the piezoelectric transducer.

and a thickness of $0.25mm$ is placed in the middle of the plate. The transducer is adhesively bonded on the rear surface of the structure. This configuration enables laser scanning of a flat front surface. Two damages in form of $40mm$ long and $1mm$ wide cuts have been introduced at different spatial positions and different orientation with respect to the transducer, see Figure 4. The excitation frequency of the voltage pulse is $90kHz$, because here the amplitude ratio between the A_0-mode and S_0-mode is maximized, compare [28].

The proposed laser vibrometry setup is only sensitive to out-of-plane deformation, because the laser beam strikes the plate orthogonally. At a frequency-thickness product of $135kHz{\cdot}mm$ the out-of-plane motion of the S_0-mode is too small to be measured. Consequently, the following experimental analysis is solely based on the A_0-mode. At each spatial position of the structure the measurement is repeated ten times in order to improve the signal-to-noise ratio. The underlying grid has a spatial sampling of Δx=$3mm$. Having recorded all the time-traces it is possible to create an image for each time step.

5. Results

The described software system was implemented in C++ using OpenGL and GLSL/Cg (shader model 3, [29]). We have evaluated the system on different hardware platforms comprising commodity graphics notebooks and workstations. The performance measurements refer to a commodity system with an Intel Core2Duo $2{,}4GHz$ (P8600), 4GB RAM, GeForce 9600mGT, and Windows 7 $64bit$ operating system.

As an example, the simulated plate shown in Figure 2a was modeled using a subdivision into 71x36 spectral elements. In the simulation part, the computation of one time step of the displacement field (see Section 3.1) took an average of 3.8 milliseconds. An overall number of 7832 time steps were computed. To ensure an interactive feedback while jumping back and forth in time, every $150th$ time step was cached in a 3D texture (see Section 3.2). On all tested platforms, the GPU-based approach allows us to visualize the Lamb wave propagation at frame rates significantly higher than the display rate of a standard computer display (60Hz-100Hz).

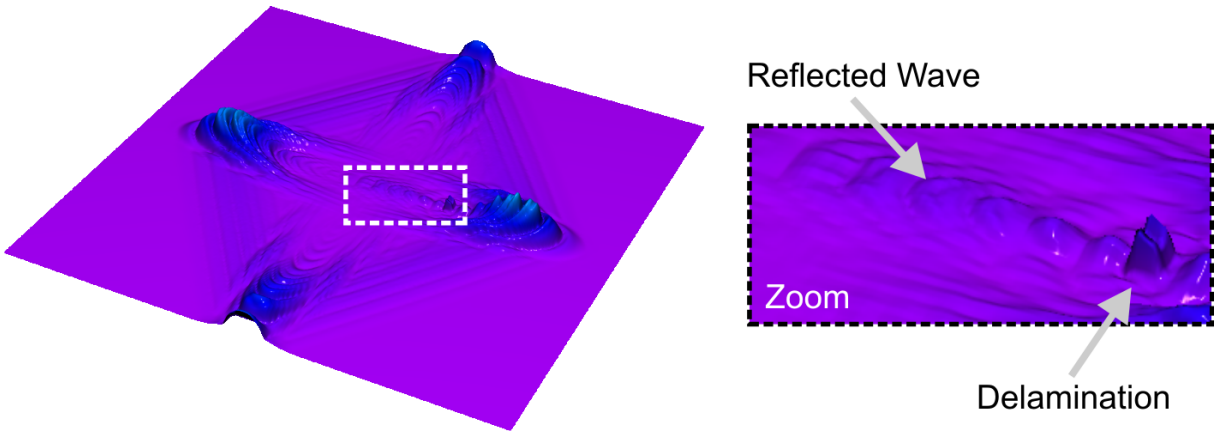

Figure 5. Wave propagation of the in-plane motion in an anisotropic plate. The wave velocity depends on the direction of propagation and the peak-to-peak amplitude is significantly higher in fiber direction than e.g. in 45 degree direction. The incident wave is reflected at the delamination and much energy is concentrated in the delaminated region.

Figure 5 shows a snapshot of the simulated in-plane wave-field in a squared anisotropic plate. In contrast to the wave propagation in isotropic material the wave velocity is here a function of the propagation direction. This can be observed in Figure 5, where the wave packets in the one direction have already reached the boundaries while in the other direction there is some space between the wave packets and the plate boundaries. Due to the higher stiffness in fiber direction the peak-to-peak amplitude is significantly higher in fiber direction than e.g. in 45 degree direction. Damage has been simulated in form of a non-penetrating delamination. Thanks to the visualization it can be observed that the incident wave is reflected at the delamination. The reflected wave has the greatest amplitude in fiber direction. Furthermore, it can be concluded from Figure 5 that major energy portions remain inside the delaminated region. This is because the ultrasonic waves are multiple times reflected from one end to the other end of the delamination, while only little energy leaves the delamination.

Figure 6 shows the out-of-plane wave-field of the plate from Figure 4 recorded by the laser vibrometry system after $30\mu s$. The top left of this figure uses the radio-frequency signals while Figure 4b is based on the Hilbert envelope of the ultrasonic signals. In both cases it can be clearly seen that the amplitudes of the reflected waves depend highly on the orientation of the synthetic cut and the position of the transducer. In case of the cut that is situated on the lower right of the plate the incident ultrasonic wave strikes the long side of the cut almost orthogonally. Consequently, most of the energy is reflected in the normal direction of this cut. In case of the second cut, the amplitude is much lower and has less angular dependency. Here, the incident ultrasonic wave hits the defect at the tip where the reflection coefficient is relatively small. It can be concluded from these results that the visualization provides detailed information about the scattering properties at the defect.

Further information about the acoustic wave-field can be solely seen by the visualization technique that is based on the Hilbert envelope. Although the plate is isotropic and the transducer has a circular shape, the amplitudes are higher in horizontal and lower in vertical direction. This effect can be referred to the bending dynamics of the piezoelectric disc [30]. Additionally, this visualization technique shows the shape of the synthetic cut, see Figure 4c with the correct orientation of the reflector. Another interesting information can be seen in Figure 4d that shows the wave-field at $26\mu s$. Due to the fact that the cut covers the total

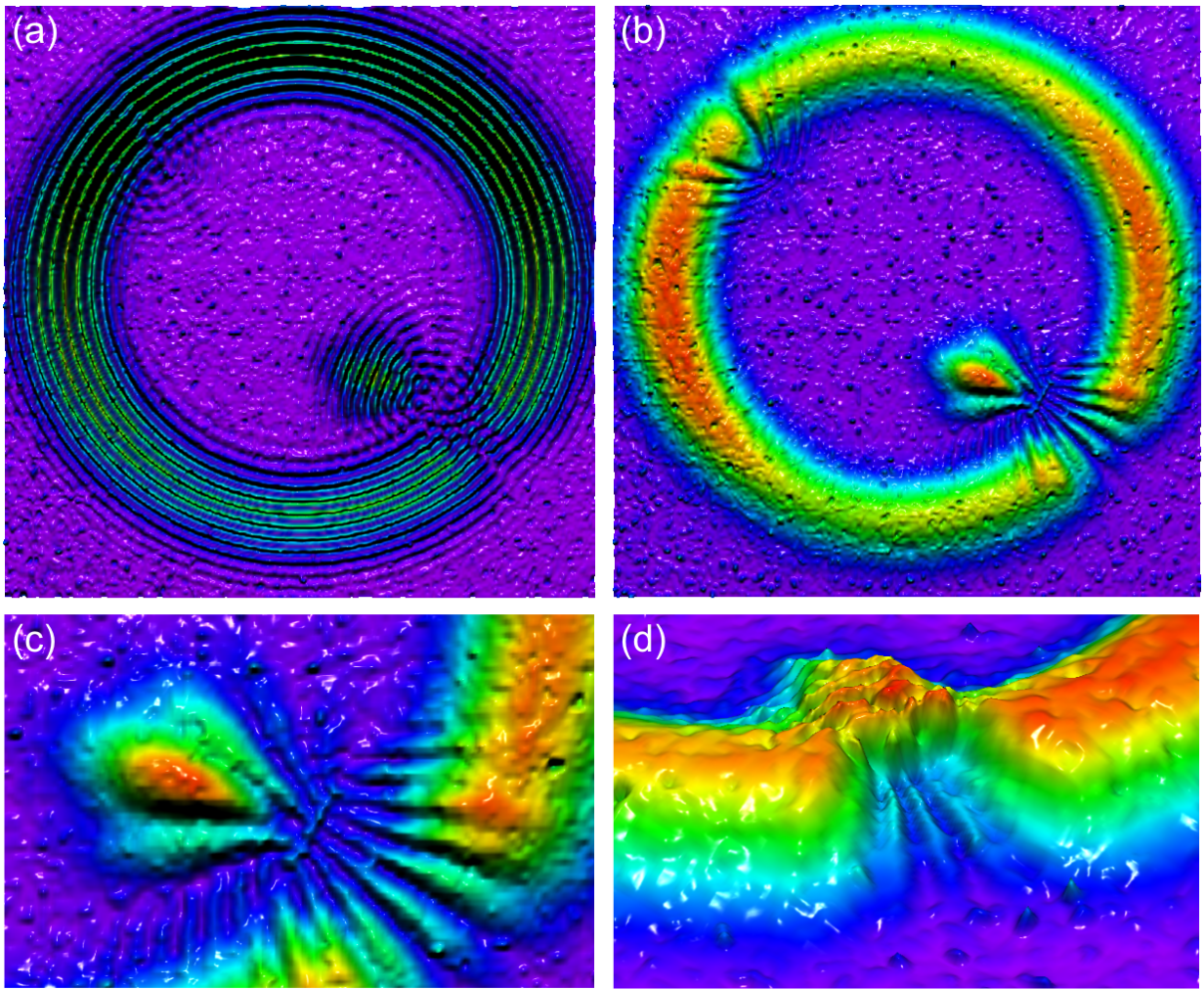

Figure 6. (a) Visualization based on radio-frequency signals (b) Visualization based on envelope-detected signals (c) close-up of the scatterer showing its shape and orientation (d) accumulation of the ultrasonic waves in front of the defect.

cross-section of the plate, the ultrasonic waves cannot pass the obstacle and accumulates right in front of the defect.

6. Discussion

Besides the valuable information provided by the visualization, the high computing rates of the GPU implementation enable the optimization of sensor positions. This process is very important to enhance the information about potential structural defects. One possible measure of a proper sensor configuration might be the probability of detection. This statistical quantity evaluates how probable it is to recognize the damage with a certain sensor setup. The practical implementation of this approach requires the simulation to be performed multiple times for each sensor configuration which is indeed a very time-consuming task.

Although we use a 3D texture to cache the results of the spectral elements simulation, modifications applied to the basic conditions of the simulation, such as the element tessellation, the mass- and stiffness matrices or the location of the piezoelectric actuators, however, will require the cache to be invalidated and the simulation to be restarted from the beginning.

A current limitation of our system is the topology of the spectral elements. Currently, we restrict ourselves to manifold surface topologies in the simulation without bracing or supporting structures.

7. Conclusions and future work

In this paper we have presented the prototype of an integrated simulation and visualization system for structural health monitoring using Lamb waves. Such a system allows to interactively investigate the nature of Lamb wave propagation in isotropic and anisotropic materials. The benefits of the proposed SHM-system are the high computing rates that can be used to simulate wave propagation time-efficiently. Furthermore, the interactive character of the visualization supports the human perception that is more sensitive to motion than to changes in color.

As a future work we are planning to expand the system to arbitrary topologies, i.e. structural elements including strutting and bracing elements which cannot be easily described by a manifold surface topology. From the insights gained throughout our study we are planning to formulate a strategy to optimize the sensor configuration.

Acknowledgement

This work was partially supported by the *Stiftung der deutschen Wirtschaft.*

References

[1] Croxford A, Moll J, Wilcox P and Michaels J 2010 *Ultrasonics* **50** 517–528
[2] Lu Y, Lin Y, Su Z and Huang N 2007 *Smart Materials and Structures* **16** 1907–1914
[3] Moll J, Schulte R, Hartmann B, Fritzen C P and Nelles O 2010 *Smart Materials and Structures* **19**
[4] Salas K and Cesnik C 2010 *Smart Materials and Structures* **19**
[5] Graves R 1996 *Bulletin of the Seismological Society of America* **86** 1091–1106
[6] Fornberg B 1987 *Geophysics* **52** 483–501
[7] Zienkiewicz O, Taylor R L and Zhu J Z 2005 *The finite element method, 6th edition* (Elsevier Butterworth-Heinemann, Oxford)
[8] Cho Y and Rose J L 1996 *J. of the Acoustical Society of America* **99** 2079–2109
[9] Delsanto P, Schechter R S and Mignogna R B 1997 *Wave Motion* **26** 329–339
[10] Patera A 1984 *J. of Computational Physics* **54** 468–488
[11] Kudela P, Zak A, Krawczuk M and Ostachowicz W 2007 *J. of Sound and Vibration* **302** 728–745
[12] Kim Y, Ha S and Chang F K 2008 *AIAA Journal* **46** 591–600
[13] Kudela P and Ostachowicz W 2009 *7th International Conference on Modern Practice in Stress and Vibration Analysis*
[14] Schulte R, Xing K and Fritzen C P 2009 *Key Engineering Materials* vol 413-414 pp 253–260
[15] Staszewski W, Lee B, Mallet L and Scarpa F 2004 *Smart Materials and Structures* **13** 251–260
[16] Staszewski W, Mahzan S and Traynor R 2009 *Composites Science and Technology* **69** 1678–1685
[17] Ruzzene M 2007 *Smart Materials and Structures* **16** 2116–2129
[18] Schulte R and Fritzen C P 2010 *Proceedings in Applied Mathematics and Mechanics* vol 10
[19] Kudela P and Ostachowicz W 2008 *Applied Mechanics and Materials* **9** 89–104
[20] Michaels T E and Michaels J E 2006 *Review of Progress in Quantitative Nondestructive Evaluation* vol 25B pp 1484–1491
[21] Schulz M, Weiler M, Reuding T and Ertl T 1999 *Proceedings of the 6th SIAM Conference on Geometric Design*
[22] Johnson C, Parker S, Hansen C, Kindlman G and Livnat Y 2003 *IEEE Computer* **32** 59–65
[23] Reddy J 2004 *Mechanics of laminated composite plates and shells* (CRC Press)
[24] Pozrikidis C 2005 *Introduction to finite and spectral element methods using Matlab* (Chapman and Hall)
[25] Seriani G and Priolo E 1994 *Finite Elements in Analysis and Design* **16** 337–348
[26] Yang Z and Purves D 2003 *Nature Neuroscience* **6** 632–640
[27] Blinn J F 1977 *SIGGRAPH Comput. Graph.* **11**(2) 192–198
[28] Moll J and Fritzen C P 2010 *24th Conference on Noise and Vibration Engineering, Leuven, Belgium (on CD-Rom)*
[29] Rost R J 2009 *OpenGL Shading Language, 3rd edition* (Pearson Education, Inc)
[30] Huang H, Pamphile T and Derriso M 2008 *Smart Materials and Structures* **17**